PASJ: Publ. Astron. Soc. Japan **46**, L173–L177 (1994)

X-Ray Spectrum and Variability of the Quasar PG 1211+143

Tahir YAQOOB,[1*] Peter SERLEMITSOS,[1] Richard MUSHOTZKY,[1] Greg MADEJSKI,[1*] T. Jane TURNER,[1*] and Hideyo KUNIEDA[2]

[1]*NASA/Goddard Space Flight Center, Greenbelt, MD 20771, USA*
[2]*Department of Physics, School of Science, Nagoya University, Furo-cho, Chikusa-ku, Nagoya 464-01*

(Received 1994 June 3; accepted 1994 July 20)

Abstract

We present preliminary results of an ASCA observation of the classic soft-excess quasar PG 1211+143. The overall ASCA spectrum can be characterized by a blackbody with a temperature of ~ 125 eV (quasar frame) and a power law with photon index ~ 2. Simultaneous ROSAT data are suggestive of further steepening of the spectrum just below the ASCA band. Comparison with previous observations shows that the soft flux in the 0.1–2 keV band varies by at least a factor of ~ 16, scaling roughly as the square of the hard flux in the 2–10 keV band over a timescale of ~ 13.5 yr. We also find evidence of short-term amplitude variability of up to a factor ~ 2 on a timescale of $\sim 2 \times 10^4$ s, in both the soft and hard flux so that the soft and hard photons are likely to originate from the same, compact, region. The data rule out variable absorption (cold or ionized) as the origin of the soft excess, favoring an intrinsic emission component. However, we argue against optically thin emission for the 'blue bump' in PG 1211+143. The large amplitude soft X-ray variability may be indicative of variations in the effective temperature, or peak, of the soft component. There is only marginal evidence for Fe K line emission between 6–7 keV in the quasar frame.

Key words: Quasars: individual (PG 1211+143) — X-rays: galaxies — X-rays: spectra

1. Introduction

The quasar PG 1211+143 ($z = 0.085$) is a classic example of an AGN with a particularly prominent UV/soft X-ray excess, or 'big blue bump' (Bechtold et al. 1987; Elvis et al. 1991; Comastri et al. 1992; Saxton et al. 1993). The source has a moderately high luminosity (~ 1–3×10^{44} ergs s^{-1} in the 2–10 keV band) and is the only one of 33 quasars with soft X-ray spectra in the Einstein IPC survey to be dominated by an extremely steep, soft X-ray spectrum (Wilkes, Elvis 1987). Amongst a set of Einstein and EXOSAT observations, the soft flux has been observed to vary on a timescale as short as ~ 18 d (an increase by a factor of ~ 2.3) and the same data set hinted at a correlation between the soft and hard X-ray flux (Elvis et al. 1991). Despite the extensive study of soft excesses in this and many other AGN, there is still no consensus as to their origin. This has mainly been due to the lack of X-ray detectors with good resolution combined with a broad bandpass required to simultaneously characterize the soft and hard emission components. The most popular interpretation of the soft excesses still appears to be the thermal emission expected from a geometrically thin, optically thick accretion disk (possibly modified by Comptonization; e.g., see Ross et al. 1992). It has been argued by Elvis et al. (1991) that an optically thin thermal source cannot account for variability of the soft flux on the 18-day timescale mentioned above. However, it has been counter-argued that this is not true if the source consists of a large number of small emitters instead of a single, uniform emission region (Barvainis 1993). Both thin and thick (e.g., Guilbert, Rees 1988) models envisage reprocessing of hard X-rays into the bump photons but the extent of such reprocessing is at present unclear.

2. The ASCA Data

PG 1211+143 was observed by ASCA on 1993 June 3. ASCA has four identical, thin-foil, light-weight X-ray telescopes (XRT) which focus X-rays onto one of two Solid-state Imaging Spectrometers (SIS) or one of two Gas Imaging Spectrometers (GIS: see Ohashi et al. 1991). See Tanaka et al. (1994) for a summary of the ASCA mission and focal-plane detectors. The SIS sensors, each one consisting of four CCD (Charge Coupled Device) chips were operated in a mode in which all four chips were exposed (4-CCD mode). SIS data from FAINT and BRIGHT modes were combined. Only data from one

* With the Universities Space Research Association.

chip (which contains the majority of the counts) from each SIS is analysed here. Hereafter the two SIS sensors are referred to as S0 and S1 and the two GIS sensors as S2 and S3. Spectra were extracted from each sensor from a circular region centered on the source (typically 3′ in radius for the SIS and 5′ for the GIS). Background spectra were taken from annulii centered on the source but far enough away to avoid contamination from the source (suitable radii were selected by examining the radial profile). The background constitutes $\sim$ 3–4% of the total in the SIS and $\sim$ 7–9% of the total in the GIS. The duration of the observation was about 8.5×10^4 s. Data were rejected by (i) removing 'hot' and 'flickering' pixels in the SIS, (ii) examining light curves of off-source regions to select good time intervals when the background is not high and/or variable, (iii) imposing a minimum geomagnetic cut-off rigidity of 8 GeV c^{-1}, and (iv) imposing a minimum Earth elevation angle of 15° for obtaining SIS spectra and 5° for the GIS and also for SIS light curves. Method (ii) is also good for rejecting data affected by light leakage in the SIS allowing lower minimum Earth elevation angles to be used. These rather strict selection criteria gave $\sim 2.3 - 2.6 \times 10^4$ s effective exposure time for SIS spectra and $\sim 3 \times 10^4$ s for GIS spectra.

3. Light Curves

Figures 1a and 1b show the light curves from S2 and S3 respectively (in the 0.8–10 keV band), while figure 1c shows the light curve from S0 in the 0.4–2 keV band and figure 1d the light curve from S0 in the 2–10 keV band. The points in the light curve were computed from the count rates in the final, merged good time intervals after data selection so the bin size is variable, ranging from $\sim$ 300 to 2000 s. Using a fixed bin size makes it difficult to detect variability if the bins are too small and variability can be 'washed out' if the bins are too large. All the light curves in figure 1 show significant variability. In particular, the flux increases by almost a factor of 2 in $\sim 2 \times 10^4$ s near the beginning of the observation. This behavior is present in all four detectors. The soft and hard flux in S0 appears to show correlated variability in the first half of the observation but not in the second. Light curves from S1 are consistent with S0. We have checked whether the apparent variability is due to the slight variation of the source centroid on the detector focal plane (typically much less than 1′). No correlation is found between the position of the source centroid and the distance from the XRT optical axis. We also find no correlation of the variability with the small attitude variations of the satellite (up to $\sim$ 1′ in both RA and DEC). This, together with the fact that the variability is present in all detectors suggests that the observed variability is indeed due to the source. This short-term variability implies that both the soft and hard emission originates in a compact region of size $\sim 6 \times 10^{14}$ cm or less. In the optically thin scenario, the ensemble of cloudlets must be confined to this region.

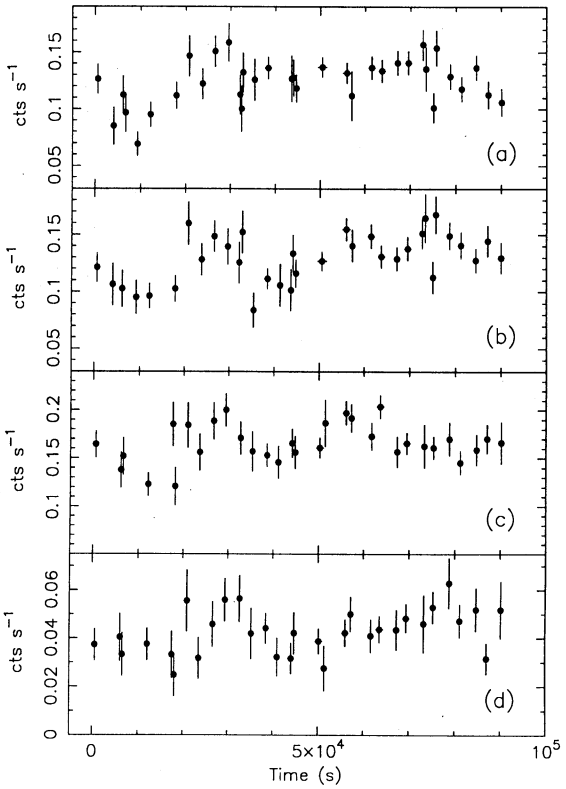

Fig. 1. (a) The 0.8–10 keV light curve from S2. (b) As (a) but for S3. (c) The 0.4–2 keV light curve from S0. (d) The 2–10 keV light curve from S0.

4. Spectral Fitting Results

In this section we bin the spectra to have a minimum of 20 counts per bin, in order to use the χ^2 statistic and apply background subtraction. We use data in the $\sim 0.4 - 10$ keV for the SIS and $\sim 0.8 - 10$ keV for the GIS. Preliminary spectral fitting showed that no simple, single component model could adequately fit the SIS spectra. A single power-law plus absorber fit gave $\chi^2 = 178.6$ (95 degrees of freedom) for S0 and $\chi^2 = 142.8$ (89 degrees of freedom) for S1, rejecting the model at greater than 99.9% confidence in both cases. Also, the best-fitting absorbing column was zero in both cases.

Next we fit the data with a power-law plus blackbody model. An absorbing column is included, fixed at the Galactic value of 2.83×10^{20} cm^{-2} (Elvis et al. 1989) and the cross-sections in Morrison and McCammon (1983) are used. The model is applied to the spectra from S0 and S1 individually, S0 and S1 simultaneously and fi-

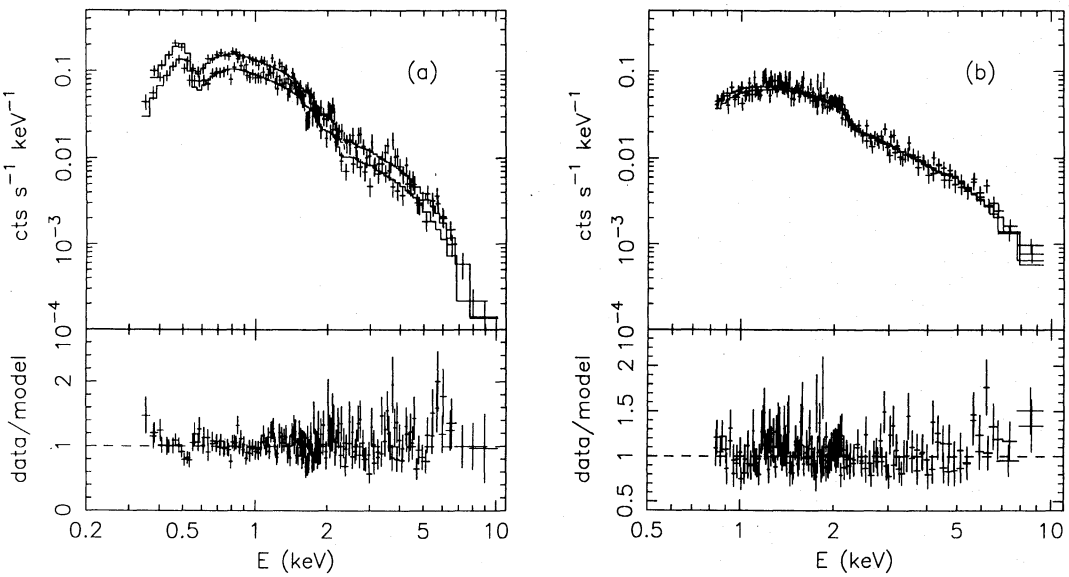

Fig. 2. The data, best-fitting power-law plus blackbody model and the ratios of data to model for the four instrument simultaneous fitting. The SIS data (a) are shown separated from the GIS data (b) for clarity.

nally, all four instruments simultaneously (S0–S3). Only the continuum normalizations are independent in the simultaneous fits. Good fits are obtained in all cases and the results are shown in table 1. The individual fits to S0 and S1 show consistent results, as do the simultaneous fits. Three instrument fits with S0, S1, and GIS spectra from either S2 or S3 also give consistent results. If we include an additional (floating) column density in any of the fits, χ^2 decreases by less than 0.01 and the additional column is always much less than 10^{19} cm^{-2}. For the four instrument fit, the data, best-fitting model and ratios of data to model are shown in figures 2a (SIS) and 2b (GIS). The best-fitting power-law index, $\Gamma \sim 2$ is consistent with previous measurements with EXOSAT (Comastri et al. 1992; Saxton et al. 1993) and Ginga (Williams et al. 1992). Comparison with previous measurements of the best-fitting blackbody temperature, $kT \sim 125$ eV, is not straight-forward due to the different column densities used in the literature and different instrumental bandpasses. A four-instrument fit with a Raymond-Smith plus power-law model gives extremely low abundances ($0.005^{+0.005}_{-0.004}$ relative to solar) due to the lack of emission lines in the spectra. The resulting quasar-frame plasma temperature from such a fit is 287^{+31}_{-17} eV. Note that no systematic errors to account for known instrumental uncertainties, of the order of $\sim 5-20\%$ at various energies, have been included in these fits. In particular, the residuals in the SIS below ~ 0.6 keV are seen in data from other sources (e.g., see Yaqoob et al. 1994).

Examination of the data to model ratios between 5–7 keV for both SIS and GIS in figure 2 shows that there

Table 1. Power law plus blackbody fits to PG 1211+143*

DET	Γ	kT (eV)	χ^2(d.o.f.)
S0.....	1.96(1.84–2.08)	126(117–136)	88.8(94)
S1.....	2.10(1.95–2.25)	124(110–137)	114.6(88)
S0,S1...	2.01(1.92–2.11)	126(118–133)	206.1(184)
All.....	2.01(1.95–2.07)	126(119–133)	491.1(476)

* Parentheses indicate 90% confidence intervals for two interesting parameters (see Lampton et al. 1976).

may be an Fe K line present in the spectrum. No instrumental effect is known which could produce these residuals (e.g., see Yaqoob et al. 1994 for a comparison with 3C 273), nor can the background account for them. If we add a Gaussian component to the power-law plus blackbody four-instrument model, with fixed center energy and intrinsic width (6.4 keV and 0.1 keV in the quasar frame, respectively) we obtain a best-fitting observed equivalent width of 198 eV (1 parameter, 90% confidence range of 55–341 eV). However, the improvement in χ^2 is only 8.8 for one additional free parameter, though this is still greater than 99% significance. Note that the ratio of line-intensity to continuum normalization is constrained to be the same for each instrument. If we let the center energy and intrinsic width float, we get best-fitting values of ~ 6.6 keV and ~ 0.48 keV respectively, though neither parameter is well-constrained.

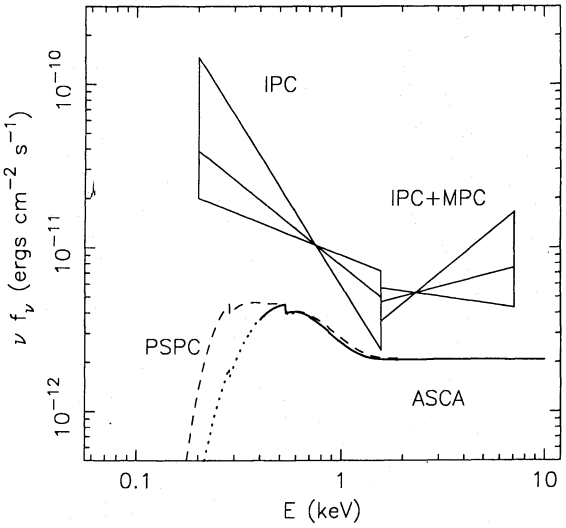

Fig. 3. Best-fitting observed models from IPC/MPC, ASCA and ROSAT data (see text). Dotted line is the extrapolated ASCA model.

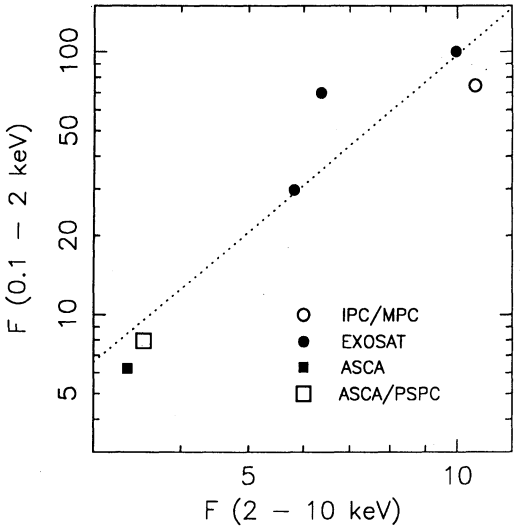

Fig. 4. The 0.1–2 keV flux plotted against the 2–10 keV flux from various instruments and the best-fitting power law, excluding PSPC data (see text). Both fluxes are in units of 10^{-12} erg cm^{-2} s^{-1}.

Further observations will be necessary to investigate the putative line-emission in order to constrain models of the central engine.

5. Spectral Variability

From the ASCA data we estimate a mean 2–10 keV flux (F_{2-10}) of 3.4×10^{-12} erg cm^{-2} s^{-1}, corresponding to a 2–10 keV *quasar-frame* luminosity of $\sim 1.1 \times 10^{44}$ erg s^{-1} ($H_0 = 50$ km s^{-1} Mpc^{-1} and $q_0 = 0$). We estimate the *extrapolated* ASCA 0.1–2 keV flux ($F_{0.1-2}$) to be $\sim 6.2 \times 10^{-12}$ erg cm^{-2} s^{-1}. Figure 3 shows the best-fitting ASCA power-law plus blackbody model, compared with the best-fitting power-law models to low-energy IPC and high-energy IPC plus MPC data from an observation in 1980 December (taken from Bechtold et al. 1987). ROSAT PSPC data, simultaneous with the latter $\sim 4 \times 10^4$ s of the ASCA observation, also exist. Simultaneous fitting of the ASCA/PSPC data requires the spectrum to be steeper below the ASCA band than spectral fitting to the ASCA data alone would suggest. For example, figure 3 (dashed line) shows the result of a five-instrument fit with two blackbodies plus a power law (mimicking a Comptonized blackbody spectrum), giving $kT_1 = 46$ eV, $kT_2 = 136$ eV, $\Gamma = 1.96$, and $\chi^2 = 565.7$ (542 d.o.f.). We stress that this does not take into account any possible temporal gain variations of the PSPC and that a full discussion of more physical models of the broadband spectrum and cross-calibration issues will be reported elsewhere. Here we simply note that, with the addition of the PSPC data, the above model gives values of $F_{0.1-2}$ and F_{2-10} of 8.0 and 3.5×10^{-12} erg cm^{-2} s^{-1} respectively. It is evident that PG 1211+143 underwent dramatic spectral and amplitude variability between the times of the IPC/MPC and ASCA observations. Figure 4 shows a plot of $F_{0.1-2}$ versus F_{2-10} from the IPC/MPC data, three EXOSAT observations (Saxton et al. 1993) and the present ASCA observation (with and without the PSPC data), spanning a total of ~ 13.5 yr. The soft flux varies by a factor of ~ 16 while the hard flux only varies by a factor of ~ 3. A linear fit of $\log(F_{0.1-2})$ versus $\log(F_{2-10})$ using the ASCA-only point gives $F_{0.1-2} = 0.56F_{2-10}^{2.24}$ and $F_{0.1-2} = 0.73F_{2-10}^{2.12}$ using the ASCA/PSPC point (the correlation coefficients are 0.93 and 0.92 respectively).

6. Conclusions

We can now rule out several alternative origins of the soft excess in PG 1211+143 which have been viable contenders in the past. First, variable cold and/or complex absorption can be eliminated as this would have been detected in the ASCA observation in which the absorption would have been largest. Warm absorber fits to the ASCA data show that the material has to be almost fully ionized. Since the ASCA data pertain to a low intensity state of PG 1211+143, the spectral change required in higher intensity states cannot be accounted for by a simple warm absorber. We have also shown that the data rule out a blend of soft X-ray lines as the dominant source of the soft excess. Thus the soft X-rays must constitute

an intrinsic emission component. Historical data spanning over a decade in the optical (Maoz et al. 1994; Yates, Garden 1989, and references therein) and UV (Bechtold et al. 1987; Walter, Courvoisier 1992) show much less than a factor of two variability. The amplitude and variability timescale of the soft X-rays, on the other hand, argue against optically thin emission for the 'blue bump'. Finally, a robust hard photon index of $\Gamma \sim 2$ in the face of large amplitude X-ray variability is consistent with both saturated 'pair-cascade' models (e.g., Zdziarski et al. 1990) and two-phase thermal Comptonization models (e.g., Haardt, Maraschi 1991). In the former, differential variability in the soft and hard X-rays is possible without a change in the effective temperature, or peak, of the seed soft photon distribution (e.g., see Yaqoob 1992) whereas the latter *does* require a change in the effective temperature in order to account for spectral variability. This is because for a given soft photon temperature and optical depth (giving a particular value of Γ) the overall spectral shape is fixed (see Haardt, Maraschi 1991).

The authors wish to thank all the members of the ASCA team who have made this work possible. TY, PJS, and RF thank the Institute of Space and Astronautical Science for their hospitality during an extended stay when part of this work was done.

References

Barvainis R. 1993, ApJ 412, 513
Bechtold J., Czerny B., Elvis M., Fabbiano G., Green R.F. 1987, ApJ 314, 699
Comastri A., Setti G., Zamorani G., Elvis M., Giommi P. 1992, ApJ 384, 62
Elvis M., Giommi P., Wilkes B.J., McDowell J. 1991, ApJ 378, 537
Elvis M., Lockman F.J., Wilkes B.J. 1989, AJ 97, 777
Guilbert P.W., Rees M.J. 1988, MNRAS 233, 475
Haardt F., Maraschi L. 1991, ApJL 380, L51
Lampton M., Margon B., Bowyer S. 1976, ApJ 208, 177
Maoz D., Smith P.S., Jannuzi B.T., Kaspi S., Netzer H. 1994, ApJ 421, 34
Morrison R., McCammon D. 1983, ApJ 270, 119
Ohashi T., Makishima K., Ishida M., Tsuru T., Tashiro M., Mihara T., Kohmura Y., Inoue H. 1991, Proc. SPIE 1549, 9
Ross R.R., Fabian A.C., Mineshige S. 1992, MNRAS 258, 189
Saxton R.D., Turner M.J.L., Williams O.R., Stewart G.C., Ohashi T., Kii T. 1993, MNRAS 262, 63
Tanaka Y., Inoue H., Holt S.S. 1994, PASJ 46, L37
Walter R., Courvoisier T.J.-L. 1992, A&A 266, 65
Wilkes B.J., Elvis M. 1987, ApJ 323, 243
Williams O.R. et al. 1992, ApJ 389, 157
Yates M.G., Garden R.P. 1989, MNRAS 241, 167
Yaqoob T. 1992, MNRAS 258, 198
Yaqoob T. et al. 1994, PASJ 46, L49
Zdziarski A.A., Ghisellini G., George I.M., Svensson R., Fabian A C., Done C. 1990, ApJL 363, L1